Phase ordering of conserved vectorial systems with field-dependent mobility

Federico Corberi*
Dipartimento di Scienze Fisiche, Università di Napoli and Istituto Nazionale di Fisica della Materia, Unità di Napoli, Mostra d'Oltremare, Padiglione 19, 80125 Napoli, Italy

Claudio Castellano†
The Abdus Salam International Center for Theoretical Physics, Strada Costiera 11, P.O. Box 586, 34100 Trieste, Italy
(Received 29 April 1998)

The dynamics of phase-separation in conserved systems with an $O(N)$ continuous symmetry is investigated in the presence of an order-parameter-dependent mobility $M\{\boldsymbol{\phi}\}=1-a\boldsymbol{\phi}^2$. The model is studied analytically in the framework of the large-N approximation and by numerical simulations of the $N=2$, $N=3$, and $N=4$ cases in $d=2$, for both critical and off-critical quenches. We show the existence of a universality class for $a=1$ characterized by a growth law of the typical length $L(t)\sim t^{1/z}$ with dynamical exponent $z=6$ as opposed to the usual value $z=4$, which is recovered for $a<1$. [S1063-651X(98)16609-6]

PACS number(s): 05.70.Fh, 64.60.Cn, 64.60.My, 64.75.+g

I. INTRODUCTION

The phase-separation kinetics of conserved systems quenched from a high-temperature disordered state into the ordered region of the phase diagram is usually modeled by the Cahn-Hilliard [1] equation for the order parameter field $\boldsymbol{\phi}(\mathbf{x},t)=\{\phi_\alpha(\mathbf{x},t)\}$ (with $\alpha=1,\ldots,N$),

$$\frac{\partial\boldsymbol{\phi}_\alpha(\mathbf{x},t)}{\partial t}=\nabla\left\{M(\boldsymbol{\phi})\nabla\left[\frac{\delta F(\boldsymbol{\phi})}{\delta\boldsymbol{\phi}_\alpha}\right]\right\}. \tag{1}$$

In Eq. (1), $F(\boldsymbol{\phi})$ represents an O(N) symmetric free-energy functional with ground state in $\boldsymbol{\phi}^2/N=(1/N)\Sigma_{\alpha=1}^{N}\phi_\alpha^2=1$ and $M(\boldsymbol{\phi})$ is the mobility. Although in the original work of Cahn and Hilliard a constant M was proposed, it has been subsequently argued [2] that, for scalar systems, a field-dependent mobility

$$M(\boldsymbol{\phi})\propto 1-a(T)\phi^2 \tag{2}$$

is more appropriate; $a(T)\to 1$ for temperature $T\to 0$, while $a(T)\to 0$ for $T\to T_c$. For vectorial systems it is natural to generalize Eq. (2), considering a mobility

$$M(\boldsymbol{\phi})\propto 1-a(T)\frac{\boldsymbol{\phi}^2}{N}. \tag{3}$$

Phase-ordering in the presence of nonconstant mobility has recently been studied with $N=1$ [3,4], showing a richer behavior with respect to the usual case with constant M. From a microscopic point of view it is easy to understand the existence of two different coarsening mechanisms in the separation of binary mixtures, which is the typical realization of a scalar conserved phase-ordering system. The first is surface diffusion, namely the diffusion of molecules along domain walls in order to minimize the interfacial energy, and is associated with a growth law of the domain size $L(t)\sim t^{1/z}$, with $z=4$. The second consists in the evaporation of molecules from large curvature regions of domain interfaces and their subsequent diffusion through the other phase towards less curved interface portions. It is often called also Lifshitz-Slyozov or evaporation-condensation mechanism; the growth exponent is $z=3$ [5]. Since bulk diffusion is an activated process and surface diffusion is not, an interesting phenomenology occurs when the temperature is changed. For high T (but still $T<T_c$), one observes only bulk diffusion ($z=3$), which is faster than the other mechanism. When the temperature is lowered, bulk diffusion is strongly suppressed due to its activated nature; it is therefore possible to observe a preasymptotic regime dominated by surface diffusion ($z=4$). This crossover is reproduced by the continuum equations with nonconstant mobility [3,4], when the parameter a is varied. At the coarse-grained level of the continuum equations, this again can be understood by observing that while for shallow quenches ($a\ll 1$) $M(\phi)$ remains finite in the whole system, the situation is different when deep quenches are considered. When $a=1$, the mobility vanishes within domains and suppresses bulk transport; since $M(\phi)\simeq 1$ on domain boundaries, the motion of interfaces is instead unaffected.

Despite the formal analogy of Eq. (1) for scalar and vectorial fields, the underlying coarsening mechanisms are in principle different, as a consequence of the different symmetry of the ground state. However, for $N\leqslant d$ one has stable localized topological defects, of which domain walls are the scalar counterpart. With constant mobility, defects play in vectorial systems exactly the same role of surfaces for $N=1$: Phase-ordering proceeds for long times by reduction in their typical radius of curvature (if they are extended) or via mutual annihilation of defect-antidefect pairs (for point defects). This analogy, however, is not complete: It is not clear what are in the vectorial case the coarsening mechanisms corresponding to surface and bulk diffusion; it is not even clear that two different mechanisms must exist at all. Furthermore, when $N>d$ no stable localized defects are present

*Electronic address: corberi@na.infn.it
†Electronic address: claudio@ictp.trieste.it

and the coarsening process has evidently a different nature, even if the growth exponent is the same.

In this paper we consider the phase-ordering kinetics of a vectorial field with a nonconstant mobility. We report results obtained numerically in $d=2$ for the case $N=2$, as a paradigm of systems with topological defects, and the cases $N=3$ and 4, where stable defects are absent. We also study analytically the soluble large-N model. Interestingly, we find that the global picture is the same from $N=2$ up to $N=\infty$, and perfectly analogous to the scalar case. More precisely, while for $a \ll 1$ the power growth law $L(t) \sim t^{1/z}$ is obeyed asymptotically with $z=4$, with $a=1$ a new value of the dynamical exponent $z=6$ is observed asymptotically, corresponding to a lower growth rate, in analogy with the case $N=1$. For $a \lesssim 1$, the $z=6$ exponent is expected to be observed preasymptotically before a crossover leads to $z=4$. These results are found both for critical and off-critical quenches.

From these results it turns out that the similarity between ordering in scalar and vectorial systems is very strong. Also for $N>1$, the dynamic exponent z is changed by the depth of the quench in the presence of a nonconstant mobility. This close analogy is not limited to fields supporting topological defects but is instead valid for any number of components of the order parameter.

The paper is organized as follows: In Sec. II the model is described; in Sec. III the solution of the large-N model is presented; in Sec. IV the results of numerical simulations of two-dimensional systems with $N=2$, $N=3$, and $N=4$ are presented and compared to the cases $N=1$ and $N=\infty$; in Sec. V we summarize the results and draw our conclusions.

II. THE MODEL

We consider a system with a vectorial order parameter $\boldsymbol{\phi}(\mathbf{x},t)$ initially prepared in a configuration sampled from a high-temperature uncorrelated state with expectation values $\langle \phi_\alpha(\mathbf{x},0)\rangle = N^{1/2} m_\alpha$ and $\langle \phi_\alpha(\mathbf{x},0)\phi_\beta(\mathbf{x}',0)\rangle = \Delta\, \delta_{\alpha\beta}\delta(\mathbf{x}-\mathbf{x}')$. For $t \geqslant 0$ the time evolution is governed by the noiseless Langevin equation (1), where $M(\boldsymbol{\phi})$ is given by Eq. (3), and $F\{\boldsymbol{\phi}\}$ is assumed in the Ginzburg-Landau form:

$$F\{\boldsymbol{\phi}\} = \int d\mathbf{x} \left[\frac{1}{2} |\nabla \boldsymbol{\phi}|^2 - \frac{1}{2}\boldsymbol{\phi}^2 + \frac{1}{4N} (\boldsymbol{\phi}^2)^2 \right]. \tag{4}$$

With these positions the equation of motion for the order parameter field reads

$$\frac{\partial \phi_\alpha(\mathbf{x},t)}{\partial t} = \nabla \left\{ \left[1 - a \frac{\boldsymbol{\phi}^2(\mathbf{x},t)}{N} \right] \nabla \left[-\nabla^2 \phi_\alpha(\mathbf{x},t) - \phi_\alpha(\mathbf{x},t) + \frac{1}{N} \boldsymbol{\phi}^2(\mathbf{x},t)\, \phi_\alpha(\mathbf{x},t) \right] \right\}. \tag{5}$$

The central quantity in the study of the dynamical process described above is the structure factor, namely the Fourier transform of the pair connected equal time correlation function, defined by

$$C_\alpha(\mathbf{k},t) = \langle \phi_\alpha(\mathbf{k},t)\, \phi_\alpha(-\mathbf{k},t)\rangle - N m_\alpha^2 \delta(\mathbf{k}). \tag{6}$$

In Eq. (6) and hereafter, $\langle\ \rangle$ means ensemble averages, that is, over the stochastic initial conditions, since Eq. (5) is deterministic. If the m_α are equal (for critical quenches) all the components of the structure factor are equivalent and the index α will be dropped.

III. THE LARGE-N MODEL

In this section we present the analytical solution of the vectorial model in the limit of an infinite number of components of the order parameter field. Although it has been shown [6] that the nature of the dynamical process is different when N is strictly infinite, the signature of this being the multiscaling symmetry obeyed by the structure factor, the global picture provided by this model is often qualitatively adequate and predicts the correct dynamical exponent z for $N>1$. Here it will be shown that the nontrivial behavior of systems with nonconstant mobility, which is due to the interplay between the different coarsening mechanisms, is fully reproduced by the large-N model.

Let us consider a process where symmetry breaking can be induced along one direction by virtue of an asymmetric initial condition

$$m_1 \neq 0, \quad m_\beta = 0 \quad \{\beta = 2, \ldots, N\}. \tag{7}$$

In the large-N limit the evolution equations for the longitudinal and transverse components of the structure factor (see the Appendix) read

$$\frac{\partial C_1(\mathbf{k},t)}{\partial t} = 2\{1 - a[S_\perp(t) + m_1^2]\} k^2 \times [-k^2 + 1 - S_\perp(t) - 3m_1^2] C_1(\mathbf{k},t), \tag{8}$$

$$\frac{\partial C_\perp(\mathbf{k},t)}{\partial t} = 2\{1 - a[S_\perp(t) + m_1^2]\} k^2 \times [-k^2 + 1 - S_\perp(t) - m_1^2] C_\perp(\mathbf{k},t), \tag{9}$$

where C_1 refers to the correlations along the symmetry breaking direction, $\alpha=1$, and $C_\perp$ is the structure factor along one of the equivalent transverse directions. $S_\perp(t)$ can be computed self-consistently through

$$S_\perp(t) = \int_{|\mathbf{k}|<q} \frac{d\mathbf{k}}{(2\pi)^d} C_\perp(\mathbf{k},t), \tag{10}$$

where q is a phenomenological ultraviolet momentum cutoff.

Equation (9) together with the self-consistency relation (10) governs the dynamics in the large-N model. These equations apply to off-critical and critical quenches ($m_1=0$) as well; in the latter case only one equation is required since Eqs. (8) and (9) coincide. Notice that Eq. (9) for $C_\perp$ does not contain C_1 and, therefore, with a high-temperature disordered initial condition $C_\perp(\mathbf{k},0)=\Delta$ can be formally integrated, yielding

$$C_\perp(\mathbf{k},t) = \Delta e^{-k^4 \Lambda^4(t) + k^2 \mathcal{L}^2(t)}, \tag{11}$$

where the lengths

$$\Lambda(t)=\left\{2\int_0^t\{1-a[S_\perp(\tau)+m_1^2]\}d\tau\right\}^{1/4}, \tag{12}$$

$$\mathcal{L}(t)=\left\{2\int_0^t\{1-S_\perp(\tau)-m_1^2\}\{1-a[S_\perp(\tau)+m_1^2]\}d\tau\right\}^{1/2} \tag{13}$$

have been introduced. For long times the structure factor is sharply peaked around

$$k_m=\frac{\mathcal{L}(t)}{\sqrt{2}\Lambda^2(t)} \tag{14}$$

allowing a saddle point evaluation of the integral over momenta in Eq. (10), which yields

$$S(t)\sim\Delta\mathcal{L}^{-d}(t)e^{\mathcal{L}^4(t)/4\Lambda^4(t)}. \tag{15}$$

For long times, convergence towards thermodynamic equilibrium requires the order parameter to approach the minimum of the local part of the free energy (4), which is for $\boldsymbol{\phi}^2=N$. Hence, setting $S_\perp(t)\simeq 1-m_1^2$ asymptotically in Eq. (15), one has

$$\Lambda(t)\simeq\frac{\mathcal{L}(t)}{[4d\ln\mathcal{L}(t)]^{1/4}}. \tag{16}$$

Two different cases must then be considered, namely, $a<1$ or $a=1$. For $a<1$, one immediately obtains from Eq. (12) $\Lambda(t)\sim t^{1/4}$, which yields $\mathcal{L}(t)\sim(t\ln t)^{1/4}$ due to Eq. (15). Hence the physical length $L(t)\sim k_m^{-1}(t)$ associated with the peak of the structure factor grows as $L(t)\sim[t/\ln(t)]^{1/4}$. With $a<1$, therefore, the asymptotic behavior is the same as for a large-N system with constant mobility [7], as expected. Notice the logarithmic correction with respect to the power-law growth obeyed by systems with finite N, which is due to the multiscaling symmetry of $C(\boldsymbol{k},t)$; the dynamical exponent $z=4$ is known to be correct for all physical vectorial systems.

Let us consider now the case $a=1$. In this case, by matching Eqs. (12), (13), and (16) one finds a different solution characterized by $\Lambda(t)\sim t^{1/6}(\ln t)^{1/12}$ and $\mathcal{L}(t)\sim t^{1/6}(\ln t)^{1/3}$, which yields $L(t)\sim(t/\ln t)^{1/6}$. With $a=1$, therefore, the vanishing of the mobility in equilibrated regions slows down the dynamics and changes z from 4 to 6, similarly to the scalar case where one goes from the Lifshitz-Slyozov evaporation condensation mechanism, associated with $z=3$, to $z=4$. It must be noticed, however, that, apart from this analogy, the physics of the coarsening process is very different due to the absence of stable topological defects for $N>d$ and there is no clear indication of the nature of the transport mechanism associated with $z=6$.

IV. SYSTEMS WITH FINITE N

In this section, we present the results of the numerical solution of Eq. (5). Our aim is to present a rather complete description of the effect of a nonconstant mobility in systems with a different number of components and to compare the results with what is known for $N=1$ and with the above discussed large-N model. In order to fulfill this program, we have chosen $d=2$ and $N=2$ or $N=3$ and 4 so that we can analyze systems with and without stable topological defects.

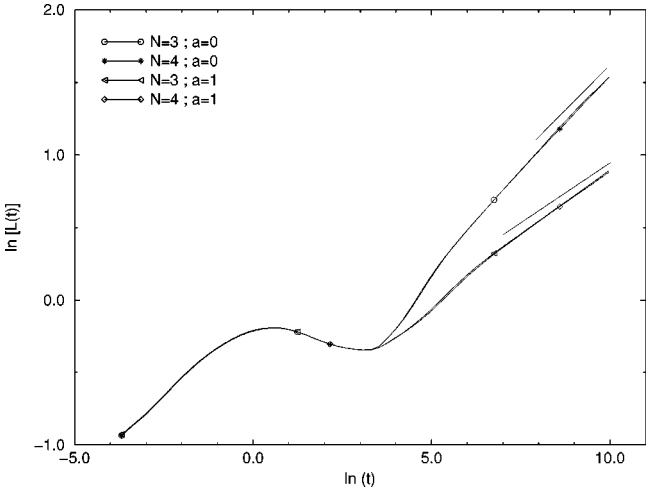

FIG. 1. The growth law of the characteristic length $L(t)$ is shown for systems with $N=3$ and $N=4$. Straight lines represent power laws $t^{1/z}$ with $z=4$ and $z=6$.

The numerical solution of Eq. (5) is obtained by simple iteration of the discretized equation on a 512×512 mesh, except for the off-critical $N=2$, $a=1$ case, which is computed on a 256×256 lattice. Each quench is averaged over three different realizations of the initial conditions. The numerical solution of Eq. (5) is particularly delicate for $a\lesssim1$, because in this case a small error in the calculation of $\boldsymbol{\phi}$ in the bulk may give rise to a negative $M(\boldsymbol{\phi})$, thus producing a spurious instability. We have avoided this problem by letting $M(\boldsymbol{\phi})=|1-a\boldsymbol{\phi}^2|$, and tested that this does not produce any significant difference in the results.

The characteristic growing length $L(t)$ is obtained from the structure factor as $L(t)=k_1^{-1}(t)$, where

$$k_1(t)=\frac{\int dk\ kC(k,t)}{\int dk\ C(k,t)} \tag{17}$$

is the first moment of $C(k,t)$.

A. $N=3$ and $N=4$

In Fig. 1, the behavior of $L(t)$ is compared in the two cases $a=0$ and $a=1$, for critical quenches with $N=3$ and $N=4$. After the linear instability is over [which corresponds to times up to $\ln(t)\simeq4$], the system enters the asymptotic regime, which is characterized by a power-law growth of $L(t)$. For $a=0$ one has $z=4$ with good accuracy almost immediately, while for $a=1$ a convergence towards $z=6$ is observed. Best-fit estimates for times larger than $t=3000$ yield $z=3.92$ and $z=3.89$ for $a=0$ and $N=3$ and $N=4$, respectively; for $a=1$, instead, one has $z=5.68$ and $z=5.81$ in the corresponding cases. We notice, by the way, the remarkable superposition of the curves with $N=3$ and $N=4$.

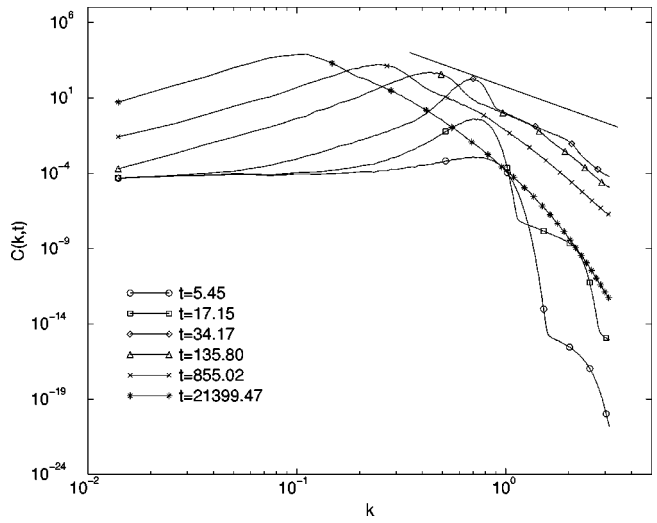

FIG. 2. The evolution of $C(\boldsymbol{k},t)$ is shown at different times for $a=0$ and $N=3$. The straight line represents a power-law decay k^{-5}.

It is interesting to observe the evolution of the structure factor, which is shown in Figs. 2 and 3, for $N=3$, at different times for $a=0$ and $a=1$, respectively. Here one observes, immediately after the linear instability corresponding to the exponential growth of a peak at constant wave vector, the formation of a rather well developed power-law decay of $C(\boldsymbol{k},t)$ for large k; this tail is initially formed at very large values of k, subsequently it moves towards lower wave vectors and then gradually disappears as time increases, being replaced by a faster (exponential) decay of the structure factor. As Fig. 2 shows, the exponent of this decay is very close to 5 in accordance with the existence of a generalized Porod's tail, i.e., $C(\boldsymbol{k},t)\sim k^{-(N+d)}$ [8]. It is well known that Porod's tail is associated with the presence of localized topological defects. The presence of such a tail in Figs. 2 and 3 suggests, therefore, that defects are formed at early time and eventually decay so that the power law disappears asymptotically. This phenomenon is displayed, with similar features,

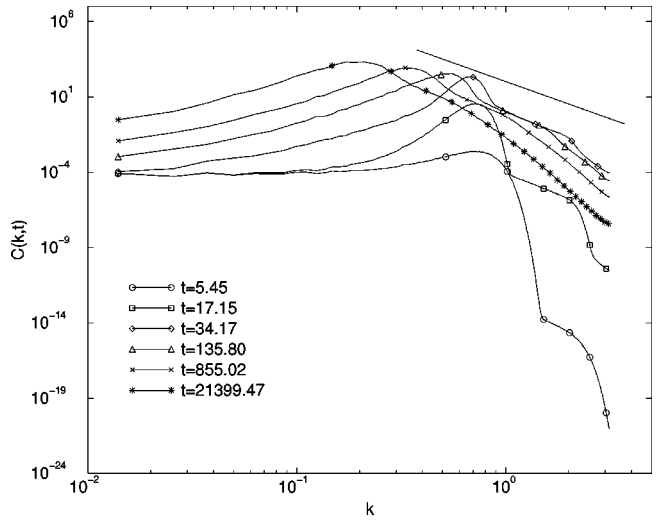

FIG. 3. The evolution of $C(\boldsymbol{k},t)$ is shown at different times for $a=1$ and $N=3$. The straight line represents a power-law decay k^{-5}.

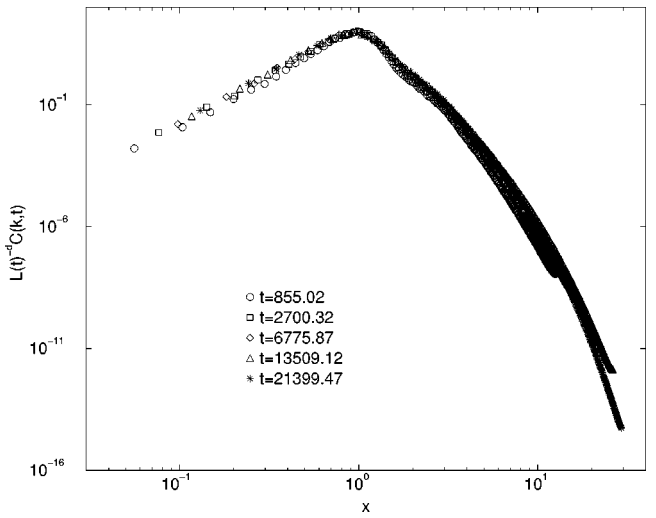

FIG. 4. Data collapse (scaling plot) for $a=0$ and $N=3$. Here $L(t)^{-d}C(\boldsymbol{k},t)$ is plotted against $x=kL(t)$ for different times.

both for $a=0$ and for $a=1$, and will be studied elsewhere [9].

In Figs. 4 and 5, the data collapse for $C(\boldsymbol{k},t)$ is presented. Here, five curves corresponding to about 1.5 decades in time are superimposed by plotting $L(t)^{-d}C(\boldsymbol{k},t)$ against $x=kL(t)$. We observe that for $a=0$ the data collapse is very good for $x\lesssim 2$, whereas it becomes progressively less accurate for increasing values of x. This effect is probably due to the remnant of the power-law tail that, for the times covered by the numerical solution, has not completely disappeared, as can be seen from Fig. 2. In any case the data are consistent with the existence of the scaling property both for $a=0$ and $a=1$. In Fig. 6, the scaling functions of the cases $a=0$ and $a=1$ are compared. The scaling function is obtained here as $L(t_M)^{-d}C(\boldsymbol{k},t_M)$, t_M being the longest time of our computation. It has been shown in [4] that no significant differences are observed in the scalar case between the two scaling functions, a fact that indicates the independence of the morphology of the growing phases with respect to a change of the coarsening mechanism from bulk to surface diffusion. Figure

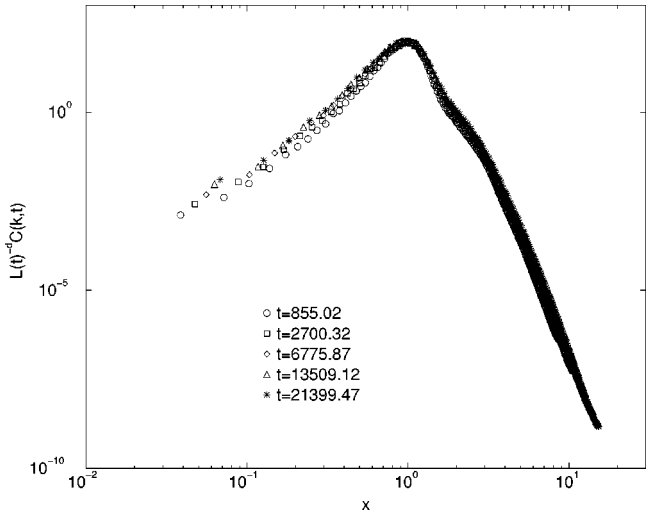

FIG. 5. Data collapse (scaling plot) for $a=1$ and $N=3$. Here $L(t)^{-d}C(\boldsymbol{k},t)$ is plotted against $x=kL(t)$ for different times.

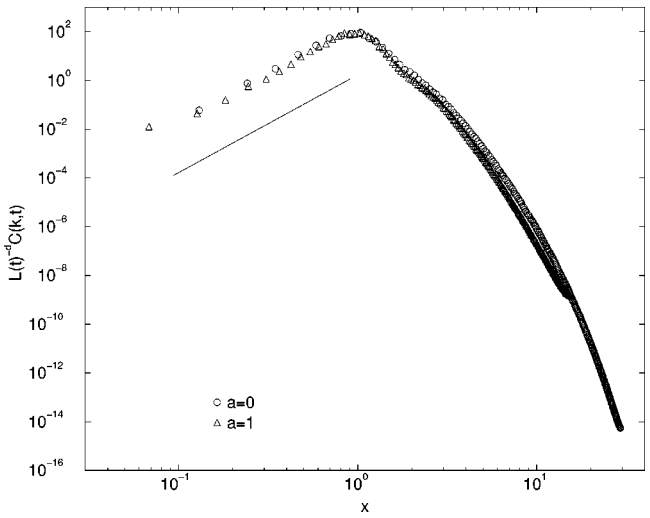

FIG. 6. Comparison between the scaling functions for $N=3$ and $a=0$ or $a=1$. The straight line represents the power law k^4.

6 shows that the same property is shared by our vectorial model. Notice also that $C(\boldsymbol{k},t)\sim k^4$ for small k [10].

B. $N=2$

We present in the following the results of the numerical simulation of the case $N=2$. In Fig. 7, the behavior of $L(t)$ is plotted versus t in the two cases $a=0$ and $a=1$. From this figure we conclude that a power-law growth with $z=4$ or $z=6$ for $a=0$ and $a=1$, respectively, fits the data very well. Linear regression analysis for $t>3000$ yields $z=4.20$ and $z=6.26$ for $a=0$ and $a=1$, respectively.

The structure factors at different times for $a=0$ and $a=1$ are shown in Figs. 8 and 9, respectively. Here one observes again the formation of Porod's tail, but, contrary to the cases $N=3$ and $N=4$, this pattern is maintained asymptotically, a fact that reflects the stability of the topological defects in the late stage of the dynamics. In Figs. 10 and 11 the scaling plots for $C(\boldsymbol{k},t)$ are presented. No compelling evidence can be obtained by the analysis of these figures

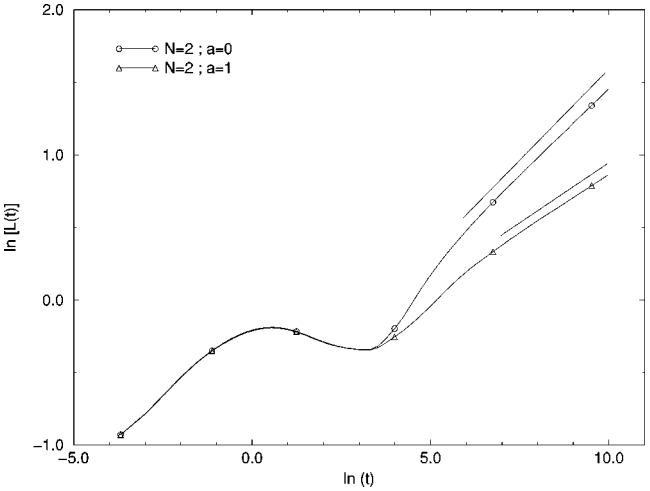

FIG. 7. The growth law of the characteristic length $L(t)$ is plotted against time for a system with $N=2$. Straight lines represent power laws $t^{1/z}$ with $z=4$ and $z=6$.

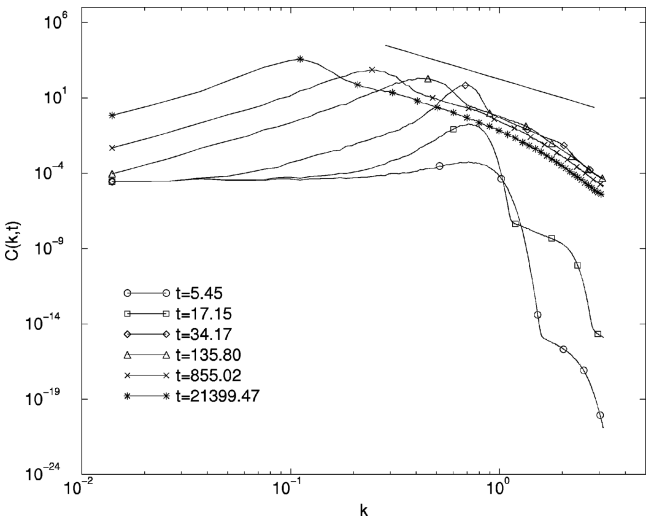

FIG. 8. The evolution of $C(\boldsymbol{k},t)$ is shown at different times for $a=0$ and $N=2$. The straight line represents a power-law decay k^{-4}.

about the possible existence of a scaling breakdown, which has been suggested with constant mobility for $d=2$ and $N=2$ [11]; nevertheless, one observes a worse data collapse with respect to the case $N=3$ and 4 for large x, both for $a=0$ and $a=1$. For $x\lesssim 2$, on the other hand, the collapse is rather good. In Fig. 12, a comparison is presented between the quantity $L(t_M)^{-d}C(\boldsymbol{k},t_M)$ (which, if scaling exists, corresponds to the scaling function) in the cases $a=0$ and $a=1$. Here one observes a superposition of the two curves for $x\lesssim 2$. For $x>2$, however, they become more and more distant with x. The situation is different from the cases $N=1$ and $N>2$ where the scaling functions practically coincide in the whole range of x values. From the observation of Figs. 10, 11, and 12 we argue that, for $x\lesssim 2$, the $N=2$ model behaves very similarly to the cases $N=1$ and $N>2$, since we find a superposition of curves at different times in the scaling plots (Figs. 10 and 11), and a very similar ''scaling function'' for $a=0$ and $a=1$. For $x>2$, however, one observes a

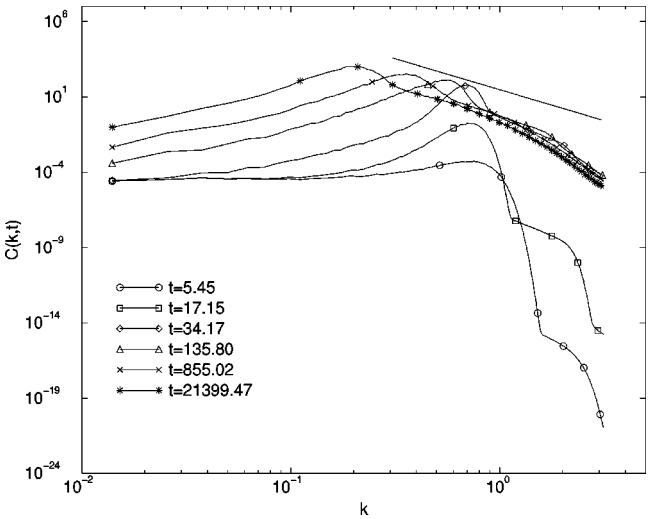

FIG. 9. The evolution of $C(\boldsymbol{k},t)$ is shown at different times for $a=1$ and $N=2$. The straight line represents a power-law decay k^{-4}.

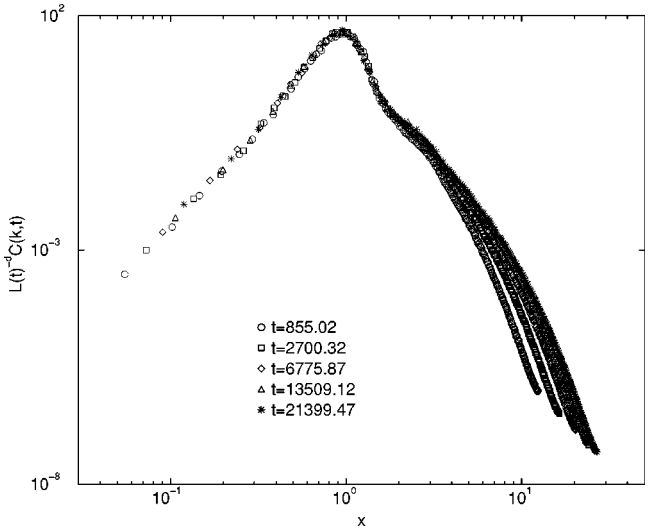

FIG. 10. Data collapse (scaling plot) for $a=0$ and $N=2$. Here $L(t)^{-d}C(\boldsymbol{k},t)$ is plotted against $x=kL(t)$ for different times.

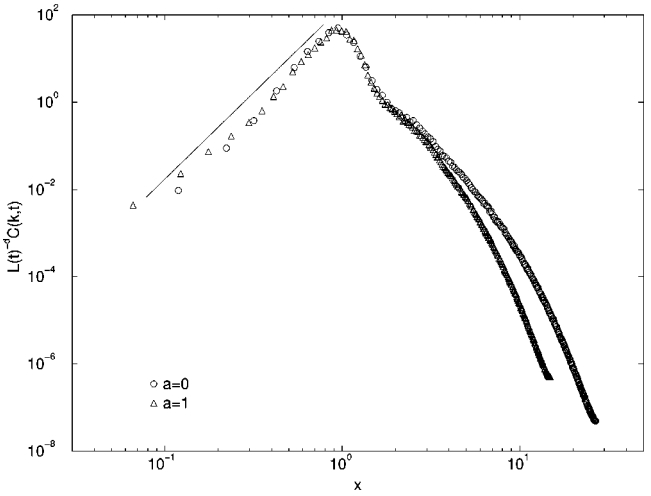

FIG. 12. Comparison between the ''scaling functions'' for $N=2$ and $a=0$ or $a=1$. The straight line represents the power law k^4.

much worse superposition in both cases. It is not presently clear if the origin of this difference is due to preasymptotic effects in the simulations or to scaling violations.

In Fig. 13, the effect of a finite m_α is considered and the growth of the characteristic length $L(t)$ is shown vs t for $a=1$ both for critical and off-critical quenches. The asymmetric quench is realized by taking $m_\alpha=0.65/\sqrt{2}$, $\forall\ \alpha$. The solution for the off-critical case has been obtained on a 256×256 lattice in order to speed up the computation since, as the figure shows, much longer times than in the critical case must be reached in order to observe the asymptotic behavior. For sufficiently long times one observes $z=6$ in both cases, suggesting that the same coarsening mechanism is at work both for critical and off-critical quenches.

V. CONCLUSIONS

In this paper we have considered the effect of an order-parameter-dependent mobility on the phase-ordering process of a vectorial system quenched in the ordered region of the phase diagram. This problem has been studied both numerically, by considering the cases $N=2$, $N=3$, and $N=4$, and analytically in the large-N limit, for critical and off-critical quenches. We have shown that for $a=1$ the dynamics is slowed down with respect to the case $a=0$, due to the vanishing of the mobility in pure phases. A power-law growth of the typical length $L(t)\sim t^{1/z}$ is still obeyed in this case but with $z=6$. This behavior is exhibited in vectorial systems for all the values of N considered and does not depend on the symmetry of the quench, nor on the presence of topological defects. We conclude that this case falls within a different universality class with respect to $a=0$. For intermediate values of a the system behaves as if $a=0$ asymptotically but a preasymptotic growth with $z=6$ is expected for a sufficiently close to 1.

These features are very reminiscent of those of scalar systems, where the dynamical exponent changes from $z=3$ to

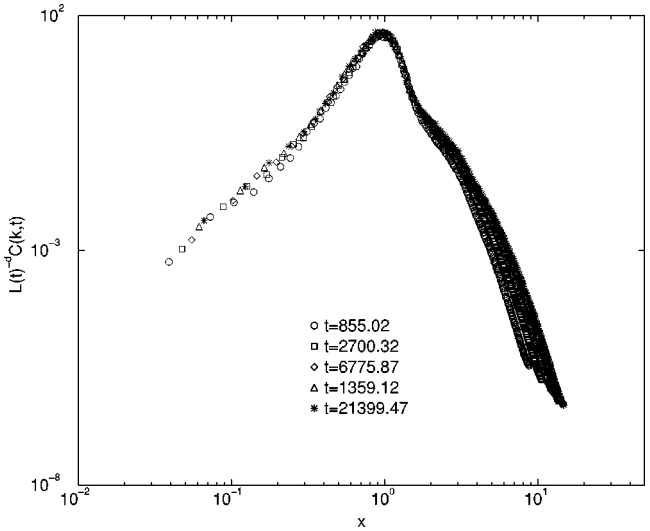

FIG. 11. Data collapse (scaling plot) for $a=1$ and $N=2$. Here $L(t)^{-d}C(\boldsymbol{k},t)$ is plotted against $x=kL(t)$ for different times.

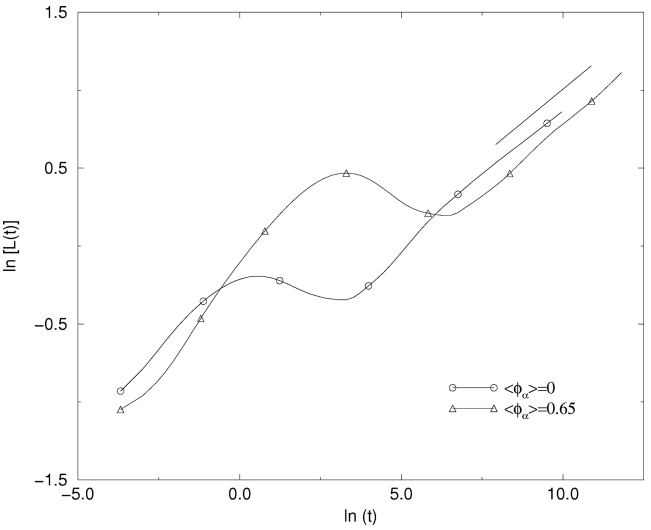

FIG. 13. The growth law of the characteristic length $L(t)$ is plotted vs t for a system with $N=2$, for $a=1$, for critical and off-critical quenches. The straight line represents the power law $t^{1/z}$ with $z=6$.

$z=4$ when $a=1$. It is, however, important to point out that the scalar models studied in Refs. [3] and [4] are not perfectly equivalent. The difference is in the form of the free-energy functional, which is of the Ginzburg-Landau type (quartic polynomial) in Ref. [3] and of logarithmic type in [4]. While the polynomial can be seen as the expansion of the logarithmic form for T not too far from T_c, for lower temperatures only the logarithmic form provides a correct coarse-grained description of the microscopic dynamics. This is confirmed by what happens for off-critical quenches to $T=0$. When the quench is sufficiently asymmetric so that the minority phase forms a nonpercolating pattern of isolated droplets, surface diffusion alone cannot drive the phase-separation to completion. The system therefore remains pinned in a configuration out of equilibrium. This pinning is correctly reproduced by the continuum equation with the logarithmic free energy [12]; no such pinning is found with the quartic polynomial [13]. In this last case the deep off-critical condition has only the effect of changing bulk diffusion to a slower mechanism ($z=4$), which has been referred to as bulk subdiffusion. The dynamical exponent for bulk subdiffusion turns out to be the same as that for surface diffusion: We do not know whether this equality is accidental or has a deeper meaning.

In our study we have considered the generalization to a vectorial order parameter of the model with Ginzburg-Landau free energy. Also in this case we find two universality classes for $a=1$ and $a<1$. This is perfectly analogous to what happens in the scalar case. Moreover, the scaling functions for $a=0$ and $a=1$ are identical. This leads us to conjecture that a mechanism of the same nature drives phase-ordering for all values of a. The only special feature of the $a=1$ case is that the mechanism is slowed down, exactly as for $N=1$ one goes from bulk diffusion to bulk subdiffusion, but the nature of the mechanism is still of bulk type.

It would be interesting to check whether a sort of generalized surface diffusion exists for $N>1$. This could be detected by solving the equation of motion for $a=1$ with a logarithmic free energy for a vectorial order parameter. An indication that this could be the case is provided by the analytical solution of the large-N model with a logarithmic form of the free energy [14].

ACKNOWLEDGMENTS

F.C. is very grateful to M. Cirillo for his hospitality. We thank C. Emmott for her useful remarks.

APPENDIX

Defining the fluctuation field $\psi(\boldsymbol{x},t)$ as

$$\phi_1(\boldsymbol{x},t)=N^{1/2}m_1+\psi(\boldsymbol{x},t) \tag{A1}$$

and inserting into Eq. (5), one obtains the pair of equations

$$\frac{\partial[N^{1/2}m_1+\psi(\boldsymbol{x},t)]}{\partial t}=\nabla\Bigg[\left\{1-a\left(\frac{1}{N}\sum_{\beta=2}^{N}\phi_\beta^2(\boldsymbol{x},t)+m_1^2+\psi^2(\boldsymbol{x},t)+2N^{-1/2}m_1\psi(\boldsymbol{x},t)\right)\right\}$$
$$\times\nabla\Bigg\{-\nabla^2\psi(\boldsymbol{x},t)-N^{1/2}m_1-\psi(\boldsymbol{x},t)+\frac{1}{N}[N^{1/2}m_1+\psi(\boldsymbol{x},t)]\sum_{\beta=2}^{N}\phi_\beta^2(\boldsymbol{x},t)$$
$$+N^{1/2}m_1^3+3m_1^2\psi(\boldsymbol{x},t)+\frac{3}{N^{1/2}}m_1\psi^2(\boldsymbol{x},t)+\frac{1}{N}\psi^3(\boldsymbol{x},t)\Bigg\}\Bigg], \tag{A2}$$

$$\frac{\partial[\phi_\beta(\boldsymbol{x},t)]}{\partial t}=\nabla\Bigg[\left\{1-a\left(\frac{1}{N}\sum_{\beta=2}^{N}\phi_\beta^2(\boldsymbol{x},t)+m_1^2+\psi^2(\boldsymbol{x},t)+2N^{-1/2}m_1\psi(\boldsymbol{x},t)\right)\right\}$$
$$\times\nabla\Bigg\{-\nabla^2\phi_\beta(\boldsymbol{x},t)-\phi_\beta(\boldsymbol{x},t)+\frac{1}{N}\sum_{\alpha=2}^{N}\phi_\alpha^2(\boldsymbol{x},t)\phi_\beta(\boldsymbol{x},t)+\left(m_1^2+\frac{2}{N^{1/2}}m_1\psi(\boldsymbol{x},t)+\frac{1}{N}\psi^2(\boldsymbol{x},t)\right)\phi_\beta(\boldsymbol{x},t)\Bigg\}\Bigg] \tag{A3}$$

with $\beta\neq 1$.

In the large-N limit, summing over vector components averages the system over an ensemble of configurations and hence

$$\lim_{N\to\infty}\frac{1}{N}|\boldsymbol{\phi}(\boldsymbol{x},t)|^2=\lim_{N\to\infty}\frac{1}{N}\sum_{\beta=2}^{N}\phi_\beta^2(\boldsymbol{x},t)=\langle\phi_\beta^2(\boldsymbol{x},t)\rangle\equiv S_\perp(t), \tag{A4}$$

where translational invariance has been assumed and $S_\perp(t)$ does not depend on β due to the internal symmetry. To leading order in N one obtains

$$\frac{\partial\psi(\boldsymbol{x},t)}{\partial t}=\{1-a[S_\perp(t)+m_1^2]\}\nabla^2\{[-\nabla^2-1+S_\perp(t)+3m_1^2]\psi(\boldsymbol{x},t)\}, \tag{A5}$$

$$\frac{\partial \phi_\beta(\boldsymbol{x},t)}{\partial t} = \{1 - a[S_\perp(t) + m_1^2]\} k^2 \{[-\nabla^2 - 1 + S_\perp(t) + m_1^2]\phi_\beta(\boldsymbol{x},t)\}. \tag{A6}$$

Introducing the longitudinal and transverse part of the structure factor, namely $C_1(k,t) = \langle \psi(\boldsymbol{k},t)\psi(-\boldsymbol{k},t)\rangle$ and $C_\perp(k,t) = \langle \phi_\beta(\boldsymbol{k},t)\phi_\beta(-\boldsymbol{k},t)\rangle$, which is independent of β due to internal symmetry and Fourier transforming, one obtains the following pair of equations:

$$\frac{\partial C_1(\boldsymbol{k},t)}{\partial t} = 2\{1 - a[S_\perp(t) + m_1^2]\} k^2 [-k^2 + 1 - S_\perp(t) - 3m_1^2] C_1(\boldsymbol{k},t), \tag{A7}$$

$$\frac{\partial C_\perp(\boldsymbol{k},t)}{\partial t} = 2\{1 - a[S_\perp(t) + m_1^2]\} k^2 [-k^2 + 1 - S_\perp(t) - m_1^2] C_\perp(\boldsymbol{k},t). \tag{A8}$$

[1] J. W. Cahn and J. E. Hilliard, J. Chem. Phys. **28**, 258 (1958); J. W. Cahn, Acta Metall. **9**, 795 (1961); Trans. Metall. Soc. AIME **242**, 166 (1968); H. E. Cook, Acta Metall. **18**, 297 (1970).

[2] K. Kitahara and M. Imada, Prog. Theor. Phys. Suppl. **64**, 65 (1978); J. S. Langer, M. Baron, and H. D. Miller, Phys. Rev. A **11**, 1417 (1975).

[3] A. M. Lacasta, A. Hernández-Machado, J. M. Sancho, and R. Toral, Phys. Rev. B **45**, 5276 (1992).

[4] S. Puri, A. J. Bray, and J. L. Lebowitz, Phys. Rev. E **56**, 758 (1997).

[5] I. M. Lifshitz and V. V. Slyozov, J. Phys. Chem. Solids **19**, 35 (1961); C. Wagner, Z. Elektrochem. **65**, 581 (1961).

[6] C. Castellano, F. Corberi, and M. Zannetti, Phys. Rev. E **56**, 4973 (1997).

[7] A. Coniglio, P. Ruggiero, and M. Zannetti, Phys. Rev. E **50**, 1046 (1994).

[8] A. J. Bray and S. Puri, Phys. Rev. Lett. **67**, 2670 (1991); H. Toyoki, Phys. Rev. B **45**, 1965 (1992).

[9] C. Castellano, F. Corberi, and M. Zannetti (unpublished).

[10] C. Yeung, Phys. Rev. Lett. **61**, 1135 (1988).

[11] A. J. Bray, Adv. Phys. **43**, 357 (1994).

[12] C. Castellano and F. Corberi (unpublished).

[13] A. J. Bray and C. L. Emmott, Phys. Rev. B **52**, 685 (1995).

[14] C. Castellano and F. Corberi, Phys. Rev. E **57**, 672 (1998).